

Proposal of wind vector estimation using observer for multi-directional propellers drone

Manto Kamiya* Student Member, Sakahisa Nagai* Member
Hiroshi Fujimoto* Senior Member, Kojiro Suzuki* Non-member

Demand for a large-size multi-rotor Unmanned Aerial Vehicle (UAV) in industrial fields is increasing and the force control of multi-rotor UAVs will be important when a UAV interacts with the surrounding environment. Multi-directional propellers drone which is generally referred to as fully actuated UAV or six degrees of freedom (DOF) UAV is receiving interest as one of the suitable UAVs for force control. Wind disturbance is one of the difficulties of force control of multi-rotor UAVs and it is important to separate the force caused by wind from others to recognize non-wind force by estimating wind vector. However, conventional methods to estimate wind vectors have difficulty distinguishing force by wind and non-wind force without additional equipment. In this study, a new observer-based method of wind vector estimation for large industrial multi-directional drones is proposed. The method uses the relationship between the counter torque of propellers and wind velocity. The counter torque of propellers is estimated by the observer. The effectiveness of the proposed method is confirmed by simulations and experiments.

Keywords: drone, multi-directional propellers drone, wind vector estimation, observer, sensorless

1. Introduction

Recently, the demand for large-size multi-rotor UAVs has been increasing in industrial fields to obtain the following two advantages⁽¹⁾⁽²⁾. First of all, a large multi-rotor UAV is capable of lifting heavy payloads, such as large cargo or heavy equipment for inspection. In addition, according to the momentum theory, it is efficient to use large propellers with low rotational speed to generate thrust.

Conventionally, multi-rotor UAVs have been mainly used to take aerial images or to carry packages with one multi-rotor UAV. On the other hand, the demand for applications of multi-rotor UAVs to interact with the surrounding environment will increase in the future. For example, it is considered to use multi-rotor UAVs for cooperative payload transportation⁽³⁾ or hammering test on buildings and bridges⁽⁴⁾. When multi-rotor UAVs conduct such missions, it is effective to implement force control in multi-rotor UAVs, such as admittance control and impedance control⁽³⁾⁽⁵⁾.

1.1 Multi-directional Propellers Drone Fully actuated multi-rotor UAV or six DOF multi-rotor UAV is a drone whose propellers are oriented in different directions. These UAVs will be referred to as “multi-directional propellers (MDP) drone” in this paper. MDP drone is currently receiving interest as one of the suitable UAVs for high-precision applications, including force control. Since a multi-rotor UAV with parallel propellers is an underactuated system, it is impossible to control six DOF simultaneously. On the other hand, as shown in Fig. 1, mounting propellers in different directions allows the drones to control their six DOF sepa-

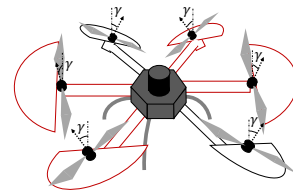


Fig. 1. Multi-directional propellers drone.

rately⁽⁶⁾⁽⁷⁾. This means that an MDP drone is able to achieve translational motion without tilting its body. Taking advantage of this feature, an MDP drone is expected to be used when force control is required, such as contact inspections⁽⁸⁾.

1.2 Wind Vector Estimation by Multi-rotor UAV

One of the significant difficulties of force control for outdoor multi-rotor UAVs is wind disturbance. The force caused by a wind disturbance should be separated from others to recognize non-wind force accurately and to implement force control. Hence, it is important to estimate a wind vector that flows into the multi-rotor UAV to distinguish the force caused by wind and non-wind force.

Some methods were proposed to date to estimate wind vectors with multi-rotor UAVs,

- Wind vector estimation by using external wrench estimation with an Inertial Measurement Unit (IMU)⁽⁹⁾
- Wind vector estimation by using the relationship between a tilt angle and wind velocity with an IMU⁽¹⁰⁾
- Wind vector measurement by using an anemometer⁽¹¹⁾

The external force applied to the body frame of multi-rotor UAVs is basically considered as a wind disturbance in the first method. The wind vector is then estimated from the relationship between wind velocity and force applied by the

* The University of Tokyo
5-1-5, Kashiwanoha, Kashiwa, Chiba, 277-8561, Japan

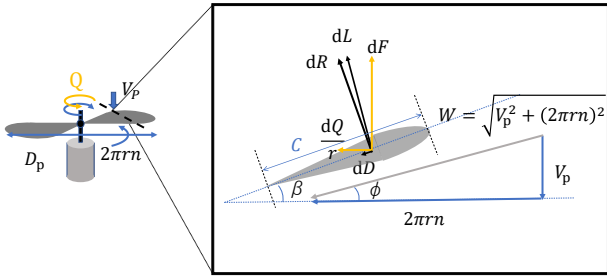


Fig. 2. Velocities and force acting on propeller blade element.

wind which is obtained experimentally or theoretically. This method is able to estimate wind vectors accurately. However, it is not easy to distinguish the force caused by wind and non-wind force. The second method uses attitude estimation by using acceleration and angular velocity obtained from IMU. The wind vector is estimated by combining velocity information obtained from Global Positioning System (GPS) and attitude information obtained from IMU. This method is also able to estimate wind vectors accurately. However, in addition to the difficulty in distinguishing force caused by wind and non-wind force, there are disadvantages such as the difficulty of synchronizing sensors. The third method is able to measure wind vectors accurately and it is also possible to distinguish force caused by wind and non-wind force. However, an anemometer increases the load and cost of a UAV.

1.3 About This Study The conventional methods of wind vector estimation have difficulty in separating force caused by wind and non-wind force without additional equipment. The purpose of this paper is to propose a method of wind vector estimation for industrial large-size MDP drones which requires no additional equipment to distinguish force caused by wind and non-wind force.

This paper is organized as follows: Section 2 describes the modeling of a propeller. A method of the angle of attack estimation for aircraft is introduced as a previous study⁽¹²⁾ and the new wind vector estimation method is proposed in Section 3. Simulations are shown in Section 4. Finally, the experiments are discussed in Sections 5 and 6.

2. Modeling of Motor and Propeller

In this section, the dynamics of the motor and propeller are focused on. The dynamics of the propeller is described with blade element theory.

The equation of motion of the electric motor is described as follows:

$$T^* - Q = 2\pi J_\omega \frac{dn}{dt} + 2\pi B_\omega n + T_c, \dots (1)$$

where T^* is torque reference, J_ω is inertia moment of propeller, B_ω is viscosity coefficient of propeller, and T_c is coulomb friction. Q is counter torque which is applied in the opposite direction of propeller rotation by the wind. n is the rotational speed of the propeller. Thrust F and counter torque Q of the propeller are described as follows:

$$F = C_F(J)\rho n^2 D_p^4, \dots (2)$$

$$Q = C_Q(J)\rho n^2 D_p^5, \dots (3)$$

ρ is air density and D_p is the propeller diameter. C_F is coefficient of thrust and C_Q is coefficient of torque. C_F and C_Q are often described as a function of advance ratio J which is defined as

$$J = \frac{V_p}{nD_p}, \dots (4)$$

The relationship between thrust F , counter torque Q and wind velocity V_p , which flows into the propeller, is explained by blade element theory. Figure 2 shows force and wind velocities acting on the propeller blade element. The blade element is the part which is r away from the center and has a thickness of dr . According to Fig. 2, dL and dD are lift and drag acting on the blade element. dL and dD are calculated by

$$dL = \frac{1}{2}\rho C_L c dr W^2, \dots (5)$$

$$dD = \frac{1}{2}\rho C_D c dr W^2, \dots (6)$$

where

$$W = \sqrt{V_p^2 + (2\pi rn)^2}, \dots (7)$$

c is the chord length, C_L is the lift coefficient, and C_D is the drag coefficient. Therefore, thrust dF and counter torque dQ of the blade element is described as follows:

$$dF = dL \cos \phi - dD \sin \phi, \dots (8)$$

$$dQ = r dL \sin \phi + r dD \cos \phi, \dots (9)$$

Let B be the number of the blades, the total thrust F and the total counter torque Q of the propeller is described as follows:

$$F = B \int dF = B \int (dL \cos \phi - dD \sin \phi), \dots (10)$$

$$Q = B \int dQ = B \int r(dL \sin \phi + dD \cos \phi), \dots (11)$$

According to Fig. 2, ϕ is determined by the ratio of V_p to the air velocity flowing laterally into the blades. Thus ϕ is obtained as

$$\tan \phi = \frac{V_p}{2\pi nr} = \frac{J}{\pi \frac{2r}{D_p}}, \dots (12)$$

According to (5)–(11), the total thrust F and total counter torque Q are calculated by integrating (10) and (11) with respect to r . Therefore C_F and C_Q are considered as a function of J .

3. Proposal of Wind Vector Estimation for MDP Drone

In this section, the wind vector estimation method for MDP drones using counter torque observer is proposed. The observer-based angle of attack estimation for electric vertical take-off and landing aircraft (eVTOL) has been proposed in ref. (12). In ref. (12), airflow angle and magnitude were estimated by using the information of a propeller and a pitot tube which is a kind of anemometer.

MDP drones have the following challenging differences compared to eVTOL. Firstly, it is not common for multi-rotor

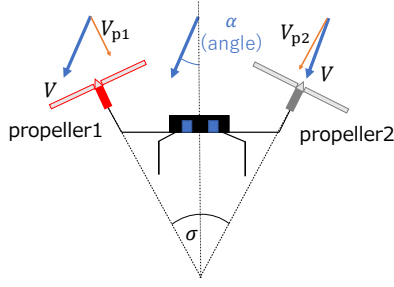


Fig. 3. Configuration of propellers of MDP drone.

UAVs to equip a pitot tube. Secondly, airspeed for an MDP drone is not as high as an eVTOL, which makes it more difficult to estimate wind velocity. This paper extends the method to multi propeller system without a pitot tube and applies it to an MDP drone. This method is based on propeller dynamics and estimates wind vectors directly. Wind affects propeller dynamics directly while propeller dynamics is less affected by non-wind force. Therefore, effects caused by wind and others can be separated by the method of this paper. The proposed method requires a degree of freedom in the direction of propellers. Therefore, large-size industrial MDP drones are the application targets in this paper. As shown in Fig. 3, the case of two propellers is considered in this paper to simplify the situation.

The proposed method estimates the velocities of airflow through the propellers by using an observer at the first step. Then, the wind vector through the body of the MDP drone is estimated by using the recursive least-squares (RLS) method at the last step. The overall estimation block diagram is shown in Fig. 4.

3.1 Airflow Velocity Estimation In the first step, the observer-based V_p estimation method is proposed. The block diagram of angular velocity ω and counter torque Q observer is shown in Fig. 5. Note that H in Fig. 5 is observer gain and I is motor current. Rotational speed n and counter torque Q are considered as the state variables and the state space equation is described as follows:

$$\dot{x} = Ax + BI, \quad n = Cx, \quad \dots \quad (13)$$

where A , B , C and x is defined as follows:

$$A = \begin{pmatrix} -\frac{B_\omega}{J_\omega} & -\frac{1}{J_\omega} \\ 0 & 0 \end{pmatrix}, \quad B = \begin{pmatrix} \frac{K}{J_\omega} \\ 0 \end{pmatrix}, \quad C = \begin{pmatrix} \frac{1}{2\pi} & 0 \end{pmatrix}, \quad (14)$$

$$x = \begin{pmatrix} \omega \\ Q \end{pmatrix}. \quad \dots \quad (15)$$

The motor torque is accurately estimated from the motor current and thus, the effects of V_p are estimated from the information of the motor current and propeller model. The thrust control of propellers which uses this fact is proposed by ref. (13). The idea of airspeed estimation using motor torque is proposed in ref. (14) and adapted to the observer-based estimation scheme in ref. (15). From (13), Q is estimated as a disturbance of the motor by using observer⁽¹⁶⁾. C_Q usually has an inverse function of J in the operating region. Therefore, V_p of each two propellers is designated by estimated Q

as follows:

$$\hat{V}_{p1} = n_1 D_{p1} C_{Q1}^{-1} \left(\frac{\hat{Q}_1}{\rho n_1^2 D_{p1}^5} \right), \quad \dots \quad (16)$$

$$\hat{V}_{p2} = n_2 D_{p2} C_{Q2}^{-1} \left(\frac{\hat{Q}_2}{\rho n_2^2 D_{p2}^5} \right). \quad \dots \quad (17)$$

As shown in Fig. 3, V_{p1} is V_p of propeller 1 and V_{p2} is V_p of propeller 2.

3.2 Wind Vector Estimation Wind vector is estimated by using the estimated \hat{V}_{p1} and \hat{V}_{p2} . It is considered that the case where V flows in at an angle of a to the propeller. As shown in Fig. 3, V_p is considered as an orthogonal component of V and V_p/V is basically described as a cosine function. However, the error which cannot be explained only by the orthogonal component appears in the actual experimental measurement⁽¹⁷⁾. Therefore, in this paper, the angular sensitivity of V_p to V is experimentally obtained as follows:

$$\frac{V_p}{V} = \cos(wa + \psi), \quad \dots \quad (18)$$

where w and ψ are fitting parameters. Therefore, V_{p1} and V_{p2} in Figs. 3 and 4 are calculated by

$$\frac{V_{p1}}{V} = \cos\left(w\left(\frac{\sigma}{2} + \alpha\right) + \psi\right), \quad \dots \quad (19)$$

$$\frac{V_{p2}}{V} = \cos\left(w\left(\frac{\sigma}{2} - \alpha\right) + \psi\right). \quad \dots \quad (20)$$

Note that σ is a predefined and fixed parameter⁽⁶⁾⁽⁷⁾. As a next step to estimate airflow angle, RLS is used by transforming (19) and (20) into the following equation:

$$Y = \eta\theta, \quad \dots \quad (21)$$

where Y , η and θ is defined as follows:

$$Y = (\hat{V}_{p2} - \hat{V}_{p1}) \cos\left(\frac{w\sigma}{2} + \psi\right), \quad \dots \quad (22)$$

$$\eta = (\hat{V}_{p1} + \hat{V}_{p2}) \sin\left(\frac{w\sigma}{2} + \psi\right), \quad \dots \quad (23)$$

$$\theta = \tan(wa). \quad \dots \quad (24)$$

Considering the conditions which are specific to multi-rotor UAVs mentioned at the beginning of the section, updating rules of RLS are divided into two cases to avoid zero dividing when η is almost zero. Updating rules of parameters is written as

$$\hat{\theta}[k] = \begin{cases} \hat{\theta}[k-1] + \frac{P[k-1]\eta[k]}{\lambda + P[k-1]\eta^2[k]} \varepsilon[k] & (|\eta| > \delta) \\ \hat{\theta}[k-1] & (|\eta| \leq \delta) \end{cases}, \quad \dots \quad (25)$$

$$\varepsilon[k] = y[k] - \eta[k]\hat{\theta}[k-1], \quad \dots \quad (26)$$

$$P[k] = \begin{cases} \frac{1}{\lambda} \left(P[k-1] - \frac{P^2[k-1]\eta^2[k]}{\lambda + P[k-1]\eta^2[k]} \right) & (|\eta| > \delta) \\ P[k-1] & (|\eta| \leq \delta) \end{cases}. \quad \dots \quad (27)$$

Note that δ is a parameter determined from the noise magnitude.

Finally, airflow angle $\hat{a}[k]$ is estimated by

$$\hat{a}[k] = \frac{1}{w} \arctan \hat{\theta}[k]. \quad \dots \quad (28)$$

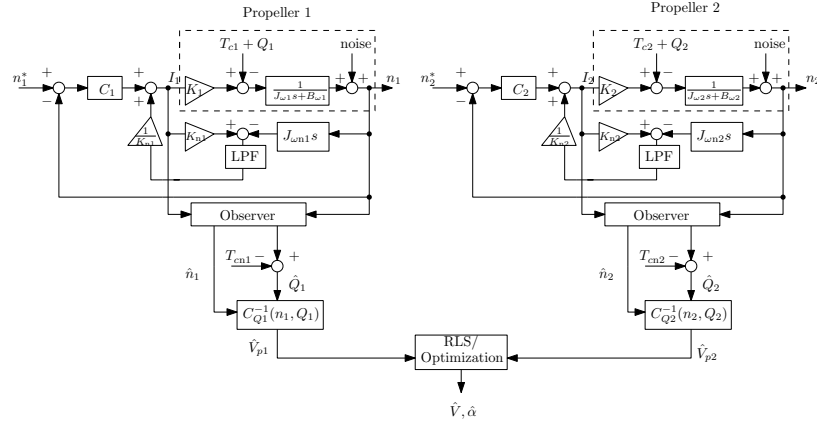


Fig. 4. Wind vector estimator.

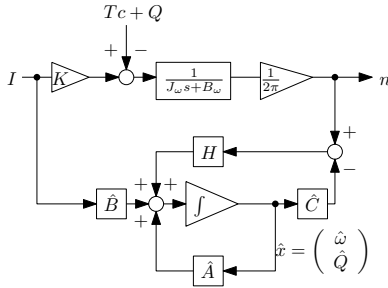


Fig. 5. Full order observer.

Table 1. Parameter in the simulation.

Symbol	Definition	Value
$J_{\omega 1}$	Inertia moment of propeller 1	$7.2 \times 10^{-5} \text{ kgms}^2$
$J_{\omega 2}$	Inertia moment of propeller 2	$1.0 \times 10^{-4} \text{ kgms}^2$
$B_{\omega 1}$	Viscosity coefficient of propeller 1	$6.0 \times 10^{-6} \text{ Nms/rad}$
$B_{\omega 2}$	Viscosity coefficient of propeller 2	$1.7 \times 10^{-6} \text{ Nms/rad}$
T_{c1}	Coulomb friction of motor 1	$1.5 \times 10^{-3} \text{ Nm}$
T_{c2}	Coulomb friction of motor 2	$3.8 \times 10^{-3} \text{ Nm}$
K	Torque constant	$30.2 \times 10^{-3} \text{ Nm/A}$
D_p	Propeller diameter	0.2 m
ρ	Air density	1.2 kg/m^3
σ	Angle between two propellers	51.3 deg
λ	Weighting factor of RLS (Sampling period 1 ms)	0.995
δ	Threshold of RLS	0.5

The airflow velocity V is estimated by

$$\hat{V} = \frac{1}{2} \left(\frac{\hat{V}_{p1}}{\cos\left(w\left(\frac{\sigma}{2} + \hat{\alpha}\right) + \psi\right)} + \frac{\hat{V}_{p2}}{\cos\left(w\left(\frac{\sigma}{2} - \hat{\alpha}\right) + \psi\right)} \right). \quad (29)$$

4. Simulation

A simulation is conducted to verify the proposed method. To simplify the situation, the simulation is run with two propellers. The wind velocity V is 5 m/s and the wind starts to flow at 2 s in the simulation. The accuracy of the method decreases when the wind velocity is low. From the point of view of force control, low wind velocity is not considered because it does not have much influence on a drone body. The airflow interference of propellers is also not considered in this paper. The airflow angle varies 10 deg to 15 deg at 6 s. The poles of observer for ω and Q of both propellers are 12 rad/s and 105 rad/s, respectively. The function of C_Q and the function of the angular sensitivity of V_p to V , which are based on ex-

perimental data, are shown in Figs. 6(a)–6(c). Each value of data samples in Figs. 6(a) and 6(b) is the average of the measurements over a three-second period. Each value of data samples in Fig. 6(c) is the average of the measurements over the five-second period at 1800 rpm. Both function of C_Q and function of the angular sensitivity of V_p to V are measured under the wind velocity of 5 m/s. In addition, each value of C_Q is measured by changing the rotational speed of propeller n . Other conditions of simulations are shown in Table 1.

4.1 Estimation of Airflow Velocity Flowing in Propellers Fig. 7(a) shows the results of the V_p estimation of each propeller. As shown in Fig. 7(a), it is confirmed that the velocity of the airflow into the propeller is estimated for both propeller 1 and propeller 2. The delay of the estimation is adjusted by the poles of the observer.

4.2 Estimation of Wind Vector Figs. 7(b) and 7(c) show the results of the estimation of wind velocity V and airflow angle of wind α . As shown in Figs. 7(b) and 7(c), it is confirmed that the proposed method is able to estimate the wind velocity and airflow angle of the wind. Note that the airflow angle cannot be defined during the period of time from 0 s to 2 s because no airflow is flowing in. The delay of the estimation of α is adjusted by λ of RLS.

5. Experiment

In order to validate the effectiveness of the proposed method, experiments in the wind tunnel are conducted. To simplify the situation, the experiments were conducted with two propellers.

5.1 Experimental Setup The experimental conditions are the same as in Table 1. The rotational speed of the propeller is 2500 rpm. The experiment at 15 deg is also conducted at 4800 rpm to study the effect of varying the rotational speed. The poles of observer for ω and Q are 12 rad/s and 105 rad/s. Fig. 8 shows a picture of the experimental setup. The function of C_Q in Figs. 6(a) and 6(b) and the function of the angular sensitivity of V_p to V in Fig. 6(c) are used. Static wind vector is estimated in the wind tunnel and only airflow from the front of the propellers is assumed in this experiment. Measurements are taken at airflow angles of 15, 30, and 60 degrees, respectively. The value of the pitot tube measured at the start of the experiment is used as the true value of wind velocity. APC 9x8E-3 propeller, Maxon DC motor, Maxon 10 bit encoder, and Maxon motor driver ES-

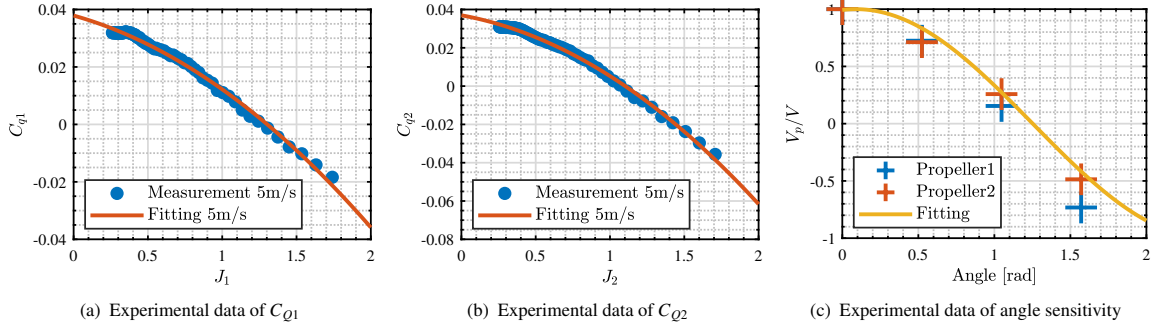


Fig. 6. Experimental data of propeller characteristics.

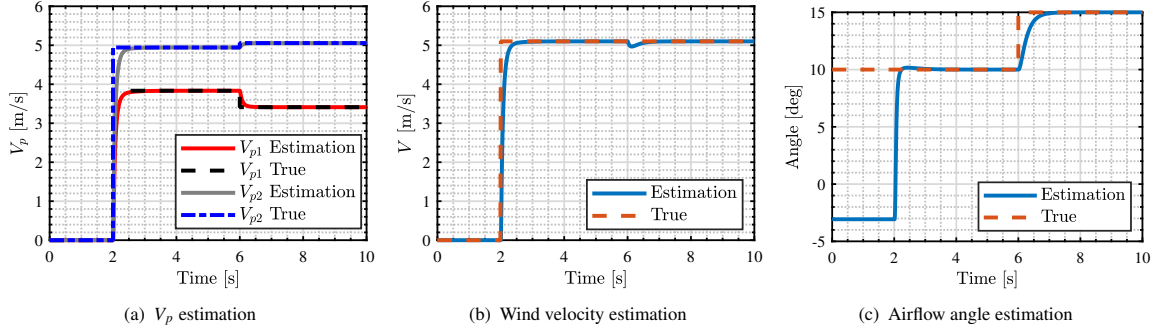


Fig. 7. Simulation of wind vector estimation.

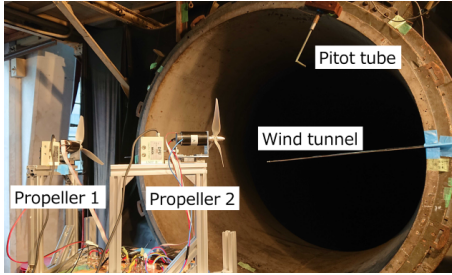


Fig. 8. Experimental setup of multi-directional propellers system and wind tunnel.

CON70/10 are used.

5.2 Experimental Result of Wind Vector Estimation

The wind tunnel test results of wind velocity estimation at each airflow angle and the results of airflow angle estimation are shown in Figs. 9–11. Estimated wind velocity is filtered by a band stop filter whose cut-off frequency is the harmonic frequency of propeller rotational speed. From Figs. 9–11, it is shown that wind vector estimation is achieved. Although C_Q is a dimensionless quantity and it is measured in advance, errors can occur due to the external environment such as temperature and humidity. According to Figs. 6(a)–6(b), the order of C_Q is 0.01. Therefore, when the value of C_Q deviates by 0.001, the maximum error of angle estimation and velocity estimation is about 6 degrees and 0.5 m/s in the simulation when 5 m/s wind flows in with airflow angle 0 to 60 degrees. Those errors can be seen in Fig. 10(c) and Fig. 11(c). Each maximum mean absolute percentage error (MAPE) of wind velocity V estimation and airflow angle α estimation of Figs. 10(a)–10(c) and Figs. 11(a)–11(c) is 9.4 % and 8.6 %. On the other hand, as shown in Figs. 10(d) and 11(d), the error of wind vector estimation is found to be large when the

rotational speed is set at 4800 rpm.

As can be seen from Figs. 6(a) and 6(b), the faster the rotational speed of the propeller, the smaller the value of C_Q varies. This phenomenon is referred to as “saturation of C_Q ” in this paper. According to (8)–(11), a saturation of C_Q occurs when the effect of the rotational speed of the propeller on Q exceeds the effect of wind velocity on Q . When this phenomenon occurs, the value of C_Q varies little with wind velocity and it makes it difficult to estimate true V_p , wind velocity V , and airflow angle α . Therefore, the cause of the large error at 4800 rpm is considered to be the saturation of the value of C_Q .

When considering the target of the method in this research, a large industrial MDP drone is expected to hover at the lower rotational speed of propellers than a small multi-rotor UAV due to the use of larger propellers. Therefore, it can be considered that saturation of C_Q is less likely to occur when a large industrial MDP drone is hovering. Even for a large industrial MDP drone, the rotational speed of the propeller must be increased during forward flight. However, the velocity of the airflow flowing into the propellers is also increased and saturation of C_Q is less likely to occur. Considering all these things, although the proposed method has a limitation of the rotational speed of the propeller, the method could be applicable to a large industrial MDP drone which is the target of this method conducting inspection on buildings or conducting cooperative payload transportation.

6. Conclusion

In this study, a new wind vector estimation method for large industrial MDP drones is proposed. The simulation and wind tunnel experiments are conducted to verify the effectiveness of the proposed method. The results of experi-

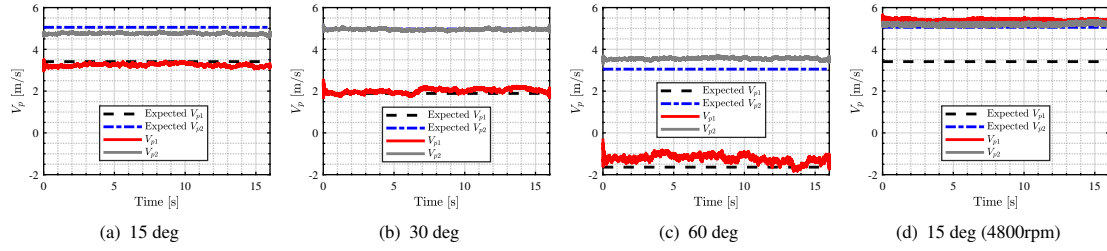


Fig. 9. Result of V_p estimation.

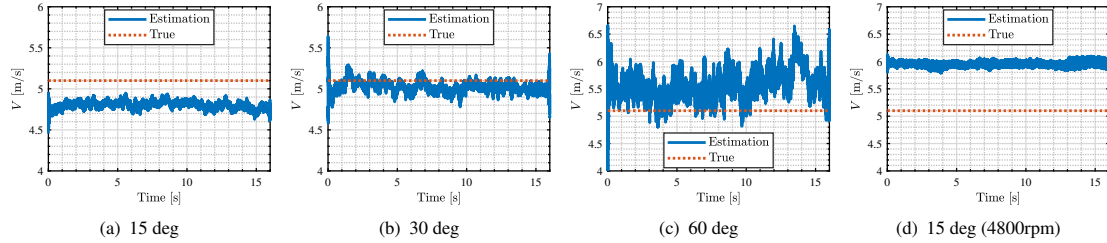


Fig. 10. Result of wind velocity V estimation.

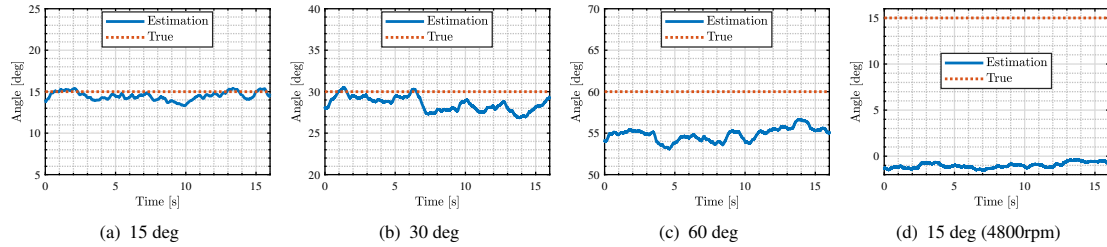


Fig. 11. Result of airflow angle α estimation.

ments indicate the usefulness of the method for large industrial MDP drones. Future work subjects include considering the airflow from the back side of propellers and reconsidering the model of propeller characteristics to improve the accuracy of wind vector estimation at the wide range of rotational speed of the propeller.

References

- (1) K. Nonami, "Research and development of drone and roadmap to evolution," *Journal of Robotics and Mechatronics*, vol. 30, no. 3, pp. 322–336, 2018.
- (2) W. Ong, S. Srigrarom, and H. Hesse, "Design methodology for heavy-lift unmanned aerial vehicles with coaxial rotors," in *AIAA Scitech 2019 Forum*, p. 2095, 2019.
- (3) A. Tagliabue, M. Kamel, S. Verling, R. Siegwart, and J. Nieto, "Collaborative transportation using mavs via passive force control," in *2017 IEEE International Conference on Robotics and Automation (ICRA)*, pp. 5766–5773, IEEE, 2017.
- (4) C. J. Salaan, K. Tadakuma, Y. Okada, Y. Sakai, K. Ohno, and S. Tadokoro, "Development and experimental validation of aerial vehicle with passive rotating shell on each rotor," *IEEE Robotics and Automation Letters*, vol. 4, no. 3, pp. 2568–2575, 2019.
- (5) Y. Nishii, D. Yashiro, K. Yubai, and S. Komada, "Design of a contact-force controller including airframe's velocity and acceleration feedback controllers for one-degree-of-freedom propeller-driven systems," *Electrical Engineering in Japan*, vol. 215, no. 2, p. e23379, 2022.
- (6) M. Ryll, G. Muscio, F. Pierri, E. Cataldi, G. Antonelli, F. Caccavale, and A. Franchi, "6d physical interaction with a fully actuated aerial robot," in *2017 IEEE International Conference on Robotics and Automation (ICRA)*, pp. 5190–5195, IEEE, 2017.
- (7) R. Rashad, J. Goerres, R. Aarts, J. B. Engelen, and S. Stramigioli, "Fully actuated multirotor uavs: A literature review," *IEEE Robotics & Automation Magazine*, vol. 27, no. 3, pp. 97–107, 2020.
- (8) R. Rashad, D. Bicego, R. Jiao, S. Sanchez-Escalonilla, and S. Stramigioli, "Towards vision-based impedance control for the contact inspection of unknown generically-shaped surfaces with a fully-actuated uav," in *2020 IEEE/RSJ International Conference on Intelligent Robots and Systems (IROS)*, pp. 1605–1612, IEEE, 2020.
- (9) T. Tomić and S. Haddadin, "Simultaneous estimation of aerodynamic and contact forces in flying robots: Applications to metric wind estimation and collision detection," in *2015 IEEE International Conference on Robotics and Automation (ICRA)*, pp. 5290–5296, IEEE, 2015.
- (10) P. P. Neumann and M. Bartholmai, "Real-time wind estimation on a micro unmanned aerial vehicle using its inertial measurement unit," *Sensors and Actuators A: Physical*, vol. 235, pp. 300–310, 2015.
- (11) A. Tagliabue, A. Paris, S. Kim, R. Kubicek, S. Bergbreiter, and J. P. How, "Touch the wind: Simultaneous airflow, drag and interaction sensing on a multirotor," in *2020 IEEE/RSJ International Conference on Intelligent Robots and Systems (IROS)*, pp. 1645–1652, IEEE, 2020.
- (12) K. Yokota, H. Fujimoto, and H. Kobayashi, "Observer-based angle of attack estimation for tilt-wing evtl aircraft," in *2021 IEEE International Conference on Mechatronics (ICM)*, pp. 1–6, IEEE, 2021.
- (13) K. Takahashi, H. Fujimoto, Y. Hori, H. Kobayashi, and A. Nishizawa, "Modeling of propeller electric airplane and thrust control using advantage of electric motor," in *2014 IEEE 13th International Workshop on Advanced Motion Control (AMC)*, pp. 482–487, IEEE, 2014.
- (14) H. Kobayashi, A. Nishizawa, and T. Iijima, "Airspeed estimation by electric propulsion system parameters," in *The 55st Aircraft Symposium*, pp. 869–878, 2017.
- (15) K. Yokota and H. Fujimoto, "Pitch angle control by regenerative air brake for electric aircraft," *IEEE Journal of Industry Applications*, vol. 11, no. 2, pp. 308–316, 2022.
- (16) K. Ohnishi, M. Shibata, and T. Murakami, "Motion control for advanced mechatronics," *IEEE/ASME transactions on mechatronics*, vol. 1, no. 1, pp. 56–67, 1996.
- (17) K. Yokota and H. Fujimoto, "Aerodynamic force control for tilt-wing evtl using airflow vector estimation," *IEEE Transactions on Transportation Electrification*, 2022.